CORE
Metadata, citation and similar papers at core.ac.uk
Provided by Nottingham ePrints

Li, Jianfeng and Agyakwa, Pearl and Johnson, Christopher Mark (2014) Suitable thicknesses of base metal and interlayer, and evolution of phases for Ag/Sn/Ag transient liquid-phase joints used for power die attachment. Journal of Electronic Materials, 43 (4). pp. 983-995. ISSN 0361-5235

Access from the University of Nottingham repository:
http://eprints.nottingham.ac.uk/36300/1/Suitable%20thicknesses%20of%20base%20metal%20and%20interlayer%2C%20and%20evolution%20of%20phases%20for%20AgSnAg%20transient%20liquid-phase%20joints%20used%20for%20power%20die%20attachment.pdf

Copyright and reuse:

The Nottingham ePrints service makes this work by researchers of the University of Nottingham available open access under the following conditions.

This article is made available under the Creative Commons Attribution licence and may be reused according to the conditions of the licence. For more details see: http://creativecommons.org/licenses/by/2.5/

A note on versions:

The version presented here may differ from the published version or from the version of record. If you wish to cite this item you are advised to consult the publisher's version. Please see the repository url above for details on accessing the published version and note that access may require a subscription.

For more information, please contact eprints@nottingham.ac.uk

Suitable thicknesses of base metal and interlayer and evolution of phases for Ag/Sn/Ag transient liquid phase joints used in power die attachment

J.F. Li*, P.A. Agyakwa, C.M. Johnson

Department of Electrical and Electronic Engineering, The University of Nottingham, University Park, Nottingham NG7 2RD, United Kingdom

Abstract

Both real Si insulated gate bipolar transistors (IGBT) with conventional Ni\Ag metallization and a dummy Si die with thickened Ni\Ag metallization have been bonded on Ag foils electroplated with 2.7 m and 6.8 m thick Sn as an interlayer at 250ºC for 0 min, 40 min and 640 min. From microstructure characterization of the resulting joints, suitable thicknesses are suggested for the Ag base metal and the Sn interlayer for Ag/Sn/Ag transient liquid phase (TLP) joints used in power die attachment, and the diffusivities of Ag and Sn in the ξAg phase are extracted. In combination with the kinetic constants of Ag_3Sn growth and diffusivities of Ag and Sn in Ag reported in the literature, the extracted diffusivities of Ag and Sn in ξAg phase are also used to simulate and predict the diffusion-controlled growth and evolution of phases in the Ag/Sn/Ag TLP joints during an extended bonding process and in service.

***Keywords*:** Transient liquid phase (TLP) bonding; Die attachment; Diffusion; Interfacial reaction; Intermetallic compounds; Solid solution

1. Introduction

* Corresponding author. Tel.: +44 115 846 6890; Fax: 44 115 951 5616.
E-mail address: Jianfeng.Li@nottingham.ac.uk

Transient liquid phase (TLP) bonding used in electronic packaging and interconnects is one of the promising alternative joining technologies for high temperature and high power density power electronics [1-4]. This is because such a TLP joint can formed through a lower melting point Sn or In interlayer, reacting with and/or diffusing into a surrounding base metal under extended isothermal solidification. The TLP bonding can hence be processed at relatively low temperatures similar to those for conventional soldering process while resulting in higher remelt temperatures of the produced joints [4]. Therefore, the TLP joints are expected to be more creep resistant and more reliable than the conventional Sn-based solder joints for applications at elevated temperatures.

As introduced in two previous papers [5,6], directed towards electronic packaging and interconnects, TLP bonding used to join base metals Ag, Au and Cu has been extensively investigated [3-13], while that to join base metals Ni, Pd, Pt and Zr has also been reported [14-16]. Within acceptable bonding temperatures and times, the produced TLP joints generally consist of intermetallic compounds (IMCs) of those base metals and Sn, In, InSn, SnBi, $BiIn_2$ or SnInBi interlayer. Despite the fact that the IMCs are more brittle than the corresponding base metals, they have much higher mechanical strength and creep resistance than the conventional Sn-based solders used in electronic packaging and interconnects. Indeed, significantly improved reliability of the TLP joint consisting of Cu_6Sn_5 and Cu_3Sn IMCs and used to attach 1200 V and 150 A Si IGBTs on a type of ceramic-based substrates had been demonstrated by means of active power cycling experiment under the maximum juncture temperatures of 165 °C to 171 °C [17].

The present work is concerned with the Ag/Sn/Ag TLP system in which the formation and evolution sequence of the intermetallic phases can be predicted using the binary Ag-Sn phase diagram as shown in Fig. 1 [18]. The feasibility of using this system for joining components for use in the high-temperature electronic industry had been proved in the late

1980s [4,7]. In a previous paper [5], the thickening kinetics of Ag_3Sn IMC growth was investigated by sandwiching a thin layer of Sn between two pieces of Ag foil at temperatures of 260 °C, 300 °C and 340 °C. In the present paper, both real Si IGBTs with conventional Ni\Ag metallization and dummy Si dice with thickened Ni\Ag metallization have been bonded on the Ag foils electroplated with 2.7 μm and 6.8 μm thick Sn as interlayer at 250 ºC for 0 min, 40 min and 640 min. Then the microstructure features in terms of phases, voids and thicknesses of the resulting joints were characterized and analyzed. The objectives of this paper are: (i) to determine suitable thicknesses of interlayer Sn and base metal Ag on both the power die and the supporting substrate for the Ag/Sn/Ag TLP system which can be used in power die attachment; (ii) to extract and report the diffusivities of Ag and Sn in ξAg IMC which are lack in the existing literature; and (iii) to simulate the diffusion-controlled growth and evolution of phases in the Ag/Sn/Ag TLP joints during extended bonding process, which can be used to predict the phases stably existing in the Ag/Sn/Ag TLP joints in service.

Given the fact that the conventional Sn-based solder joints are in general not reliable at temperatures above 125°C, the results obtained from the present work will be useful for utilizing the Ag/Sn/Ag TLP joints in the development and manufacturing of high temperature power electronic systems. For instance, it is desirable to develop power electronics modules which are reliable in continuous operation in an ambient temperature of 150 °C and above for periods of several years. Examples includes aerospace where there is an increasing move to electronic rather than hydraulic or pneumatic systems, automotive under-hood applications in conventional, hybrid and electric drive systems and down-hole gas and oil field applications. The Ag/Sn/Ag TLP joints are well suited to these applications and even able to operate at temperatures higher than the processing temperature.

2. Experimental procedure

2.1 Preparation of samples

The real Si IGBTs used in this work are 13×13×0.3 mm in size and have the conventional 0.8\0.7 μm thick Ni\Ag metallization, and the dummy Si dice are 13×13×1 mm Si chips with thickened 1\6 μm thick Ni\Ag metallization deposited using sputtering process. They were both obtained from Dynex Semiconductor Ltd (Doddington Road, Lincoln LN6 3LF, UK), and their cross-sectional scanning electronic microscopy (SEM) images are shown in Fig. 2. The as-received Ag foils electroplated with 2.7 μm and 3.1 μm, or 6.8 μm and 7.5 μm thick Sn on both sides were discs of 100 mm in diameter and 100 μm in thickness of Ag. They were obtained from Applied Materials Technology Ltd (Units 6 &7 Lyndon Business Park, Farrier Road, Lincoln LN6 3RU, UK), and their cross-sectional SEM images are given in Fig. 3.

All the samples were prepared using a sample configuration and temperature/pressure profile schematically illustrated in Fig. 4. The as-received Ag discs plated with the Sn layers were first cut into pieces of 13×13 mm in size. Then a real Si IGBT (or a dummy Si chip) was placed in contact with the surface of a 13×13 mm Ag foil plated with 2.7 μm thick Sn, and another real IGBT (or another dummy Si chip) was placed in contact with the surface of another 13×13 mm Ag foil plated with 6.8 μm thick Sn. Next, they were brought together, and put in a house-made bonding rig, where they were inserted into two ∅55×5 mm Al discs to improve the uniformity of heat delivered from both the top and bottom electrical cartridge heaters during the final bonding process. Following this, a pressure of ~2MPa was applied to the bonding area, and the samples were purged with nitrogen gas (760 mL/min at 1.5 bar). The bonding process was started by subjecting the samples to a temperature profile which involved first heating up to 200 °C at a heating rate of 45 °C/min, then heating up to 250 °C at a heating rate of 25 °C/min that the bonding rig could comfortably achieve, before holding at 250 °C for 0 min, 40 min and 640 min. Finally, the pressure was released and the samples

were taken out of the bonding rig once it cooled down to 100 °C with a time approximately of 10 min.

The combinations of Si die, Ag foil and dwelling time considered during the above bonding process and their sample codes are listed in Table I. The focus of the present work is the interfacial reactions and microstructures in the Ni/Ag/Sn/Ag and Ag/Sn/Ag/Ni parts of the bonding structure shown in Fig. 4a. The result obtained will be used to determine suitable thicknesses of interlayer Sn and base metal Ag on both the power die and the supporting substrate for the Ag/Sn/Ag TLP system which can be used in power die attachment. It should be pointed out that a certain amount of Sn was found to squeeze out of the bonding areas in all the samples of the real Si IGBTs and dummy Si chips bonded on the Ag foil plated with 6.8 μm thick Sn. However, no appreciable amount of Sn could be observed outside the bonding areas in all the samples of the real Si IGBTs and dummy Si chips bonded on the Ag foil plated with 2.7 μm thick Sn.

Metallographic cross-sections of all the bonded samples listed in Table I were prepared for the microstructural characterization and thickness measurement of the IMCs formed in the bonded samples. The samples were first mounted in epoxy resin that was cured at room temperature for 24 hours. The mounted samples were then successively ground with 800, 1000 and 1200 grit SiC papers and finally polished using diamond slurries of 3 μm and 1 μm both for 10 min.

2.2 Characterization and thickness measurement of IMCs

A JEOL 6400 SEM (JEOL Ltd, 1-2, Musashino 3-chome Akishima Tokyo 196-8558, Japan) using a backscattered electron signal was employed for the imaging and analysis of microstructural features. The IMCs formed in the bonded samples were identified using an Oxford Instruments ISIS energy-dispersive X-ray spectroscopy (EDXS) microanalysis system (Oxford Instruments plc, Tubney Woods, Abingdon, Oxfordshire OX13 5QX, UK) fitted on

the SEM. As presented in the results, from the SEM images, it is hard to determine the interface between the Ag_3Sn and ξAg IMCs even if both of them had been formed in some of the bonded samples. Therefore, the total thicknesses of the Ag_3Sn and ξAg IMCs formed in all the bonded samples and the thicknesses of the Ni_3Sn_4 IMC formed in the samples of attaching the real IGBTs were measured using an image analysis method as detailed elsewhere [5,6]. The image analysis was performed utilizing the Image Processing Toolbox Version 5.0.0 of MATLAB R14SP2 (The Mathworks, Matrix House, Cambridge Business Park, Cambridge CB4 0HH, UK). For each sample, three images 512×416 pixels in resolution, one 200×160 μm and two 40×32 μm in size, were used. A data series for the thickness of each layer in a sample was obtained from 512×3=1536 intercepted lengths in the through-thickness direction. The resulting thicknesses were given in terms of mean, standard deviation (Std. Dev.), minimum and maximum values.

In order to obtain the individual thicknesses of Ag_3Sn and ξAg IMCs formed in some of the bonded sample for extracting the diffusivities of Ag and Sn in ξAg IMC, focused ion beam (FIB) ion channelling was employed to observe the grain morphology, size and boundaries of the IMCs formed in samples C1 and C2. This was done using the FEI Quanta200 3D DualBeam FIB/SEM (FEI, Europe NanoPort, Achtseweg Noord 5, 5651 GG Eindhoven, The Netherlands) to progressively mill the polished cross sections, which provided grains and grain boundary contrast.

3. Results

3.1 Real Si IGBTs with conventional Ni\Ag metallization

There was no noticeable difference in the microstructure features of the real Si IGBTs bonded on the Ag foil plated with 2.7 μm thick Sn from those of the real IGBTs bonded on the Ag foil plated with 6.8 μm thick Sn. Fig. 5 presents the SEM images taken from the three

samples of real IGBTs bonded on the Ag foil plated with 2.7 μm thick Sn. Ag-Sn IMCs could be observed at the Ag foil side only, and the Ni barrier layer underneath the top Ag metallization of the real IGBTs had fully been reacted with Sn into Ni_3Sn_4 for all the three samples. This is quite unusual and will be further discussed in the section of discussion below.

For sample A0 bonded at 250 °C for 0 min, there was only Ag_3Sn IMC which could be detected by EDXS at the Ag foil side. There was trace Sn remaining and mixed with the Ni_3Sn_4 IMC formed at the IGBT side. For sample A1 bonded at 250 °C for 40 min, there were both Ag_3Sn and ζAg IMCs which could be identified by EDXS at the Ag foil side. It could be detected with EDXS that the Ag_3Sn IMC dominated the thickness of the Ag-Sn IMCs, but the interface between Ag_3Sn and ζAg IMCs was hard to be viewed from the SEM image. At the IGBT side, there was no appreciable pure Sn remaining any more, but there was a chain of voids of several microns in size along the interface of the Ni_3Sn_4 IMC in contact with the Ag_3Sn IMC at the Ag foil side. For sample A2 bonded at 250 °C for 640 min, there was only ζAg IMC left at the Ag foil side. The Ni_3Sn_4 IMC and a chain of voids of several microns in size formed at the IGBT side were both similar to those observed in the sample A1 bonded at 250 °C for 40 min.

The total thicknesses measured with the image analysis method for the Ag-Sn IMCs formed in all the bonded samples are listed in Table II. The means, standard deviations and maximum values for the samples A0 to A2 are almost the same as those for samples B0 to B2, respectively. The mean thicknesses for the samples A0, A1, B0 and B1 are similar to each other. This may be attributed to the Sn partially squeezed out of the bonding areas in the samples B0 and B1 that were bonded on the Ag foil plated with thicker Sn. On the other hand, the mean thicknesses for the samples A2 and B2 are clearly larger than those for the samples A0, A1, B0 and B1. This can be ascribed to the fact that the Ag_3Sn IMC formed during the

early bonding stage had been converted into ζAg IMC, which thus increased the total thickness of the Ag-Sn IMCs during the late bonding stage. In addition, the ratios of the maximum to the mean thicknesses of the Ag-Sn IMCs in the samples A0 and B0 are equal or close to 2, while those in the samples A1, A2, B1 and B2 are somewhat lower than 2.

Also measured with the image analysis method, the mean thicknesses of the Ni_3Sn_4 IMC formed at the IGBT sides were both approximately 4.0 µm for samples A0 and B0, and all in the range of 2.0 to 2.5 µm for samples A1, A2, B1 and B2.

3.2 Dummy Si Chips with thickened Ni\Ag metallization

As shown in Figs. 6 and 7, if the dummy Si chips with 1\6 µm thick Ni\Ag metallization were bonded on the Ag foil plated with 2.7 µm thick Sn, the Ni barrier layer underneath the Ag layer was intact and some residual Ag was retained at the chip side in both samples C1 and C2. For sample C1 bonded at 250 °C for 40 min, the joint mainly consisted of relatively coarse Ag_3Sn grains plus finer ζAg grains which were similar to each other at both the chip side and the Ag foil side (Fig. 7a). For sample C2 bonded at 250 °C for 640 min, the joint consisted of ζAg grains only which were also similar to each other at both the chip side and the Ag foil side (Fig. 7b).

As can be seen from Fig. 8, if the dummy Si chips with 1\6 µm thick Ni\Ag metallization were bonded on the Ag foil plated with 6.8 µm thick Sn, the Ni barrier layer underneath the Ag layer was locally attacked by Sn to produce Ni_3Sn_4 IMC at the chip side. This reveals that the liquid Sn layers in the bonding areas of these samples were somewhat thicker than those in the bonding areas of the samples C1 and C2 during the initial bonding stage. After the Ag layers on the Si chips were consumed, certain amounts of residual Sn were delivered to react with the Ni barrier layers, through the grain boundaries and/or molten channels existing between the Ag_3Sn crystals formed during the early stage. For sample D1 bonded at 250 °C for 40 min, the joint consisted of Ag_3Sn IMC plus local Ni_3Sn_4 IMC at the

chip side, and major Ag_3Sn IMC plus minor ζAg IMC at the Ag foil side. For sample D2 bonded at 250 °C for 640 min, the joint also consisted of Ag_3Sn IMC plus local Ni_3Sn_4 IMC at the chip side. However, at the Ag foil side, the joint consisted of major ζAg IMC plus minor Ag_3Sn IMC. Note that the Ag-Sn IMCs could be observed at both the Si chip side and the Ag foil side in the samples D1 and D2, which are somewhat different from those in the samples A1 and A2 where the Ag-Sn IMCs was observed at the Ag foil side only (Fig. 5).

As listed in Table II, the total thickness of the Ag-Sn IMCs formed in sample C2 is larger than that of the Ag-Sn IMCs formed in sample C1. This can be related to the change of the Ag_3Sn IMC formed during the early bonding stage into ζAg IMC during the late bonding stage. However, the total thickness of the Ag-Sn IMCs formed in sample D2 is similar to that of the Ag-Sn IMCs formed in sample D1. This may be due to the fact that different amounts of liquid Sn had partially been squeezed out of the bonding areas in samples D1 and D2 during the early bonding stage.

Comparing the total thicknesses of the Ag-Sn IMCs formed in the samples C1, C2, D1 and D2 with those formed in the samples A1, A2, B1 and B2, it can further be seen that the former values are all larger than two times of the latter values. This indicates that less amounts of Sn were available to react with Ag in the samples A1, A2, B1 and B2 than in samples C1, C2, D1 and D2. Therefore, the reaction rate of the liquid Sn with the Ni barrier layer was probably higher than that of the liquid Sn with the Ag in the samples of the real IGTBs bonded on the Ag foils.

In addition, the separate thicknesses of Ag_3Sn and ζAg IMCs formed in the sample C1 will be used to extract the diffusivities of Ag and Sn in Ag as presented below. They can be separated from the total thickness listed in Table II, with the help of the FIB image shown in Fig. 7a. The values of 5.9 μm and 2.0 μm were estimated for the thicknesses of the Ag_3Sn IMC in the middle and the ζAg IMC on both the dummy Si chip side and the Ag foil side,

respectively.

4. Discussion

4.1 Interfacial microstructure

As can be seen from Fig. 1, the solubility of Ag in liquid Sn at 250 ℃ is around 5 at%, and the amount of Ag dissolved into the liquid Sn during the bonding process should be negligible. Therefore, the result of Ag-Sn IMCs observed only at the Ag foil side in all the samples of attaching real IGBTs cannot be attributed to the dissolution of 0.7 μm Ag into the 2.7 μm (and even 6.8 μm thick) liquid Sn during the early bonding stage. More likely, this may be related to the rapid coarsening of relatively small Ag_3Sn scallops and can be explained as follows.

The effect of the initial dissolution of Ag and nucleation of Ag_3Sn may be ignored because they were extremely rapid. Following our previous work on the Ag/Sn/Ag TLP system [5], until the liquid Sn was consumed, only Ag_3Sn scallops were formed between the Sn and Ag. The evolution of the average thickness of the Ag_3Sn layer with respect to bonding time can be described using the following Eq. (1) [5]:

$$x_{Ag_3Sn} = 3..573 \times 10^3 \exp(-\frac{37.17 \pm 18.87}{RT}) t^{1/3}, \quad 0 \leq x_{Ag_3Sn} \leq x_{Ag_3Sn,\max} \qquad (1)$$

Where x_{Ag3Sn} is the average thickness of the Ag_3Sn layer in μm, t is time in s, R is the universal gas constant, T is the absolution temperature, and $x_{Ag3Sn,max}$ is maximum thickness of the Ag_3Sn layer which the Sn interlay is consumed to produce according to the reaction Eq. (2):

$$Sn + 3Ag \rightarrow Ag_3Sn \qquad (2)$$

If Eqs. (1) and (2) are extended to relatively low bonding temperature until the melting point of eutectic Sn-3.5Ag alloy, 221 ℃, they may be used to calculate the growth of the Ag_3Sn IMC and the consumptions of the Ag base metal layers and the Sn interlayer during the

early bonding stage. The calculated results for the bonding temperatures of 221 ºC and 250 ºC are shown in Fig. 9, where the densities of Sn, Ag and Ag_3Sn used during the calculation are listed in Table III. It can be seen that a layer of 0.7 µm thick Ag reacting with ~0.35 µm thick Sn (~0.7 µm thick Sn in total for two sides) produces ~1 µm thick Ag_3Sn IMC at one side of the Ag/Sn/Ag TLP sample. This takes only 2 min and 0.4 min at the bonding temperatures of 221 ºC and 250 ºC, respectively. Therefore, based on the temperature profile shown in Fig. 4b, the bonding times for the Sn interlayer to stay above the melting point should have been sufficient to consume the 0.7 µm thick Ag metallization on the all real IGBTs of the present TLP samples, even for a bonding time of 0 min at 250 ºC.

As also reported in the previous work [5], the growth of the Ag_3Sn IMC between liquid Sn and solid Ag could be well explained by the grain boundary-/molten channel-controlled growth. Once the 0.7 µm thick Ag on one IGBT was consumed, liquid Sn remaining would thus penetrate through grain boundaries between the Ag_3Sn IMC crystals to further rapidly attack and react with the Ni layer under the original Ag metallization, forming the Ni_3Sn_4 IMC at the IGBT side. With decreasing the amount of the liquid Sn, the Ag_3Sn IMC crystals or scallops formed at the two sides gradually came into contact with each other. Relatively small Ag_3Sn IMC crystals or scallops formed at the two sides tended to coalesce into relatively large Ag_3Sn scallops as they formed and grew. This was probably the reason why the Ag-Sn IMCs were observed only at the Ag foil side in all the samples of attaching real IGBTs (Fig. 4). In the samples of attaching the dummy Si chips with thickened Ag metallization, the Ag_3Sn scallops formed at the two sides had already been too large to further coarsen before they come into contact with each other. Therefore, in these samples, the Ag_3Sn scallops were observed at both the chip side and the Ag foil side (Figs. 5 and 7).

Given the fact that the average thicknesses of the Ag-Sn IMCs in samples A0, A1, B0 and B1 were all around 2 µm (Table II), it can be estimated with Eq. (2) and Fig. 9 that the

average thickness of the Ag consumed on the Ag foil side in these samples was also ~0.7 µm. The rate of the reaction between the liquid Sn and the Ag foil might be the same as or lower than that between the liquid Sn and the Ag metallization on the IGBT. Nevertheless, only ~0.7 µm thick Sn interlayer was consumed by ~0.7 µm (~1.4 µm in total for the two sides) thick Ag on both the IGBT and Ag foil sides to form the Ag_3Sn IMC (Fig. 9). More amount of the Sn interlayer, i.e. ~2.0 µm thick Sn if the Sn interlayer was 2.7 µm in thickness, was consumed by the Ni layer to produce the Ni_3Sn_4 IMC on the IGBT side in each of these samples. According to the following reaction Eq. (3):

$$4Sn + 3Ni \rightarrow Ni_3Sn_4 \quad (3)$$

With the densities of 7.36, 8.91 and 8.65 g/cm^3 for Sn, Ni and Ni_3Sn_4, the consumption of 2.0 µm thick Sn would require 0.6 µm thick Ni and produce 2.3 µm thick Ni_3Sn_4 IMC. They are in good agreement with the thickness of 0.8 µm for the Ni layer on the IGBTs and the thicknesses in the range of 2.0 to 2.5 µm for the Ni_3Sn_4 IMC formed in samples A1, A2, B1 and B2. The relatively thicker ~4.0 µm thick Ni_3Sn_4 IMC formed in samples A0 and B0 may be attributed to the existence of boundaries between the Ni_3Sn_4 IMC grains. With increasing the bonding time, the Ni_3Sn_4 IMC grains ripened and the grain boundaries migrated and developed into a chain of voids along the interface between the Ni_3Sn_4 IMC and the Ag-Sn IMCs as shown in Fig. 5. In addition, as aforementioned, the microstructural characterization and mean thicknesses of both the Ag-Sn IMCs and the Ni_3Sn_4 IMC in samples A0 to A2 were similar to those in the corresponding samples B0 to B2. This reveals that around 4 µm thick liquid Sn had probably been squeezed out of the bonding areas during the preparation of samples B0 to B2.

The solubility of Ni in liquid Sn is even lower than that of Ag at a same temperature [19]. The Ni_3Sn_4 IMC on the IGBT side should hence have been formed through the solid-liquid interfacial reaction. The solid-liquid interfacial reaction between Ni and liquid Sn to

produce Ni_3Sn_4 IMC was also reported to be grain boundary-/molten channel-controlled [20,21]. The trace Sn mixed with the Ni_3Sn_4 IMC was observed in the sample formed at 250 ºC for 0 min because it was trapped within the grain boundaries and/or molten channels. The start of the reaction of the solid Ni with the liquid Sn was later than that between the solid Ag on both the IGBT and the Ag foil sides with the liquid Sn. However, the reaction of the Ni with Sn still consumed much more amount of the liquid Sn than the reaction of the Ag with Sn. This reveals that the interfacial reaction between the liquid Sn and the Ni layer was extremely rapid when compared with that between the liquid Sn and both the Ag metallization and the Ag foil. Such a result is not in agreement with the kinetic constants for the growths of Ni_3Sn_4 and Ag_3Sn scallops reported in the existing literature [5,20,21]. This may be associated with the application of pressure in the present bonding process, but further investigation is needed to provide true understanding.

4.2 Suitable thicknesses of Ag and Sn layers for die attachment

To achieve improved reliability, the processed Ag/Sn/Ag TLP joints used in power die attachment should contain neither any Sn remaining nor any Ni_3Sn_4 IMC in contact with the Ag_3Sn IMC. This is because the Sn remaining with low melting point has relatively poor mechanical strength and creep resistance. In particular, when the operating temperature is close to and/or above the melting point, the mechanical strength of the joint will be reduced significantly or even lost. On the other hand, the ripening process of the Ni_3Sn_4 grains would lead to the formation and growth of a chain of voids between the Ag_3Sn and Ni_3Sn_4 IMCs as shown in Fig. 5, during the extended bonding stage and/or in the high temperature applications. They would not only deteriorate the thermal performance of the joints, but also act as the sites for nucleation and growth of cracks. Therefore, the existence of both the Sn remaining and the Ni_3Sn_4 IMC in contact with the Ag_3Sn IMC in the Ag/Sn/Ag TLP joints would reduce their reliability.

As mentioned previously, before the liquid Sn remaining was consumed, the thicknesses of the Ag_3Sn IMC formed and the Ag layers required to consume different thick Sn interlayers can be simply calculated with Eqs. (1) and (2). However, because of the grain boundary-/molten channel-controlled growth of the Ag_3Sn IMC between liquid Sn and solid Ag and the non-flat interfaces between the formed Ag_3Sn IMC and the residual Ag, local Ag might be consumed more and quicker than the rest of the Ag layer to react with the liquid Sn to produce Ag_3Sn IMC during the bonding process. As a result, the Ag layers to be deposited on the power die side and the substrate side as base metal layers should be thicker than those calculated according to the above reaction Eq. (2). Otherwise, once local Ag layer is consumed, Sn atoms will be rapidly delivered through the grain boundaries /molten channels existing between the Ag_3Sn crystals to attack the Ni layer and produce Ni_3Sn_4 IMC. This can be further verified by the formation of local Ni_3Sn_4 IMC in the present samples D1 and D2 as shown in Fig. 8. Despite the fact that the original thickness of the Sn interlayer in both samples was 6.8 μm, the actual thickness of the Sn interlayer in the bonding areas should be thinner than 6 μm which can approximately consume 6 μm thick Ag on both the dummy Si chip side and the Ag foil side (Fig. 9). This is because the Sn was observed to be partially squeezed out of the bonding areas in both samples during the bonding process, as aforementioned.

Again as reported in the previous paper [5], before the Ag_3Sn grains formed at the two sides of the Ag/Sn/Ag samples came into contact with each other, the ratios of the maximum to the mean values for the Ag_3Sn IMC thicknesses in the different samples were in the range of 1.9 to 2.6. Similar ratios of the maximum to the mean values for the Ag_3Sn IMC thicknesses were also observed in the present samples A0 and B0. They are in good agreement with the steady-state particle coarsening theories, which predict an upper limit on particle size about 2–2.5 times the mean particle size [20,22]. Therefore, we may consider a

factor of at least 2 to increase the thickness of the Ag layer that is needed to consume the Sn interlayer for producing Ag_3Sn IMC. This may avoid the Ni barrier layer underneath the Ag layer to be attacked by the liquid Sn during the TLP bonding process. In such a case, the thickness of the Ag layers needs to be deposited on both the power die and the supporting substrate should be at least two times the entire thickness of the Sn interlayer in the middle. For example, if the total thickness of the Sn interlayer is 2 μm, there should be at least 4 μm thick Ag layers deposited on both the power die and the supporting substrate.

Given the difficulty in depositing Ag layers thicker than 10 μm on semiconductor power devices, the Sn interlayers used for producing the Ag/Sn/Ag TL joints should generally be thinner than 5 μm. A more suitable thickness of the Sn interlayer may be 2 to 3 μm, in combination with a thickness of 4 to 6 μm for the Ag layers that are easy to be deposited on both the semiconductor power die and the supporting substrate. As demonstrated by the present result shown in Figs. 6, and 7, such a combination of the thicknesses for the Sn interlayer and the Ag base metal layers can indeed be used to produce good quality of Ag/Sn/Ag TLP joints.

4.3 Diffusivities of Ag and Sn in ξAg IMC

Before the Sn remaining was consumed, no ζAg IMC was detected in all the Ag/Sg/Ag samples reported in the previous paper [5]. We may hence assume that the ζAg IMC started to form and grow at the time when the Ag_3Sn IMC layer in the samples had already reached to its maximum thickness according to the reaction Eq. (2). Also, we may ignore the timescale for the nucleation of the ζAg crystals and assume that the thickening of the ζAg layer is diffusion-controlled at the expense of the Ag_3Sn layer formed previously. Furthermore, we may assume that the diffusion of Ag and Sn in both the ζAg IMC and Ag phases are governed by the Darken interdiffusion coefficient [23]:

$$D(N_{Sn}) = N_{Sn}D_{Sn} + (1 - N_{Sn})D_{Ag} \quad (4)$$

Where $D(N_{Sn})$ is Darken interdiffusion coefficient, N_{Sn} is Molar fraction of Sn, D_{Sn} and D_{Ag} are the diffusivities of Sn and Ag both in the ζAg IMC or both in the Ag phases. Under these assumptions, the thicknesses of the Ag_3Sn and ζAg IMCs in the present samples C1 and C2 can be used to extract the diffusivities of Ag and Sn in the ζAg IMC as described below.

First, with the kinetic constants of Ag_3Sn growth reported in the previous paper [5], if the effect of the initial dissolution of Ag and nucleation of Ag_3Sn was ignored, the evolution of the average thickness of the Ag_3Sn layer with respect to bonding time can be described using Eq. (1). Eq. (1) in combination with the reaction Eq. (2) can be used to calculate the time, t_0, when the Sn interlayer was consumed, as well as the growth of the Ag_3Sn IMC and the consumptions of the Ag base metal layers and the Sn interlayer during the early bonding stage.

Then the growth of the ζAg IMC at the expense of the Ag_3Sn IMC formed previously and subsequent evolution of the ζAg IMC with respect to bonding time can be simulated with a fixed-grid numerical method detailed elsewhere [24,25]. Essentially, this numerical method can be used to obtain the distribution and evolution of the Molar fractions, N_{Sn}, across the Ag/Sn/Ag TLP joints as schematically illustrated in Fig. 10 with respect to bonding time, based on Fick's diffusion law. The governing equations are given by:

$$\frac{\partial[N_{Sn}(x,t)/V(x,t)]}{\partial t}=\frac{\partial}{\partial x}\left[D(N_{Sn})\frac{\partial[N_{Sn}(x,t)/V(x,t)]}{\partial x}\right],\ \ S_{i-1}(t)<x<S_i(t),\ \ i=1,...,5 \tag{5}$$

$$\begin{aligned}&D_i^-(N_{Sn})\frac{\partial[N_{Sn}(x,t)/V(x,t)]}{\partial x}\bigg|_{x=S_i(t)^-}-D_i^+(N_{Sn})\frac{\partial[N_{Sn}(x,t)/V(x,t)]}{\partial x}\bigg|_{x=S_i(t)^+}\\&=[N_i^-/V_i^- - N_i^+/V_i^+]\frac{\partial S_i(t)}{\partial t},\qquad x=S_i(t),,\qquad i=1,...,4\end{aligned} \tag{6}$$

They are subject to the following boundary conditions:

$$\frac{\partial[N_{Sn}(x,t)/V(x,t)]}{\partial x}=0\qquad x=S_0(t)=L_0 \tag{7a}$$

$$\frac{\partial[N_{Sn}(x,t)/V(x,t)]}{\partial x}=0 \qquad x=S_5(t)=L_1 \tag{7b}$$

And the initial conditions can be given as:

$$N_{Sn}(x,t)/V(x,t)=N_{Sn}(x,t_0)/V(x,t_0), \quad S_0(t_0)\le x\le S_5(t_0) \tag{8}$$

Where x is position coordinate, V is Molar volume, L_0 and L_1 are two boundaries of one TLP joint, S_i $(i=1,\ldots,4)$ are moving interfaces of phases, and superscripts $^-$ and $^+$ stand for left and right sides of the moving interfaces.

In the present work, the values used in the simulation for the Molar fraction of Sn, density and Molar volume of the different phases and the interfaces in the Ag/Sn/Ag TLP joints are listed in Table III. They were calculated based on the binary Ag-Sn phase diagram and the lattice cell parameters reported in Refs. [18,26-32]. Inside each of the phases, the density and Molar volume were assumed to be linearly related to the Molar fraction of Sn. The diffusivities of Ag and Sn in Ag estimated from the Arrhenius-type plots assessed in Ref. [21] were taken as known values to calculate the Darken interdiffusion coefficient of the Ag phase. The stoichiometric width of the Ag_3Sn IMC is extremely narrow and was taken as zero, and hence the diffusion of atoms inside the Ag_3Sn layer may be ignored. Under such an assumption, the interdiffusion coefficients of the Ag_3Sn layer can be taken as any value.

Data fittings of the measured thicknesses of Ag_3Sn and ξAg layers in the samples C1 and C2 to those simulated using the numerical method to solve the above Eqs. (5) to (8) has been used to determine the diffusivities of Ag and Sn in ξAg. For each simulation, at time t_0, there are Ag_3Sn and Ag phases only in the Ag/Sn/Ag TLP joint, and their Molar fractions were set as 0.25 and 0, respectively. During the simulation, the $D(N_{Sn})$ and V dependent on the N_{Sn} were updated with an iteration method, and the calculation convergence was verified by a relative error less than 1.0×10^{-4}.

The best data fittings of the measured thicknesses of Ag_3Sn and ξAg layers in the

samples C1 and C2 to those simulated using the numerical method is plotted in Fig. 11. It can be seen that the simulated Ag_3Sn/ξAg and ξAg/Ag interfaces are in good agreement with the experimental solid points. The diffusivities of Ag and Sn in ζAg IMC at 250 °C determined from the data fittings are 5.73×10^{-16} m^2/s and 7.92×10^{-17} m^2/s as listed in Table IV. They are approximately seven and three orders of magnitude higher than those of Ag and Sn in Ag at the same temperature of 250 °C, respectively. On the other hand, they are slightly higher than the volume diffusivities of Ag and Sn in Ag_3Sn IMC, but significantly lower (four to six orders of magnitude lower) than the grain-boundary diffusivities of Ag and Sn in Ag_3Sn IMC reported in Ref. [33].

4.4 Evolution of phases during extended bonding process

With the extracted diffusivities of Ag and Sn in ζAg IMC at 250 °C, the evolution of phases in two Ag/Sn/Ag TLP joints during the extend bonding process have been simulated with the same numerical method to solve Eqs. (1) and (5) to (8). One of the joints was assumed to produce using 2 μm thick Sn interlayer sandwiched between two layers of 7 μm thick Ag base metal. The other one was assumed to produce using 4 μm thick Sn interlayer sandwiched between two layers of 14 μm thick Ag base metal. The combined thicknesses of Sn interlayer and Ag base metal layers in both simulated joints were selected for achieving the final joints consisting of the solid solution of Sn in Ag with a Sn Molar fraction of 0.0835, which is slightly lower than the equilibrium Sn Molar fraction of 0.085 at the interface of Ag in contact with ξAg IMC [18].

The simulated results are shown in Fig. 12 where the horizontal axes are in logarithmic scale. It can be seen that the timescales for consuming the Sn interlayers to produce Ag_3Sn IMC are two orders of magnitude shorter than those for consuming the Ag_3Sn IMC layers formed previously to produce ξAg IMC. Given that the fact that the initial dissolution of Ag in liquid Sn and the nucleation of Ag_3Sn crystals are even more rapid, the effect of ignoring

them during the early bonding stage on the extracted diffusivities of Ag and Sn in ζAg IMC should be negligible.

It can be noted that the ξAg IMC will continue to grow after the Ag_3Sn IMC is consumed. This can be attributed to the net diffusion of Sn atoms towards the Ag\ξAg interfaces, from the part of the ξAg IMC in the middle of the joints formed during earlier stage and with higher Molar fractions of Sn. The bonding times for consuming the Ag_3Sn IMC to produce the ξAg IMC and for consuming the ξAg IMC to form the final solid solution of Sn in Ag are 280 min and 6.5×10^9 min in Fig. 12a, and 1120 min and 2.60×10^{10} min in Fig.12b. With these timescales in mind, it is more realistic to process the Ag/Sn/Ag TLP joints consisting of major Ag_3Sn IMC plus minor ξAg IMC and residual Ag for power die attachment. Under the application environments, the temperatures can be lower than the 250 °C used in the simulation, and the evolution rates of phases in this case would be much slower than those shown in Fig. 12. Therefore, the Ag/Sn/Ag TLP joints can be expected to consist of ξAg IMC plus residual Ag during the majority of service lifetime if the Ag/Sn/Ag TLP joints are applied in power die attachment.

If the thicknesses of the Ag base metal on both the power die and the supporting substrate sides are just 2 to 2.5 times of the thickness of the entire Sn interlayer, the processed Ag/Sn/Ag TLP joints can still be expected to consist of major ξAg IMC plus minor residual Ag during the majority of service lifetime. This is because, on the one hand, under the application temperatures, the evolution rates of phases in the TLP joints should be much slower than those shown in Fig. 12. On the other hand, even if the Ag base metal layers are consumed, any possible further solid/solid interfacial reaction between ξAg IMC and Ni barrier layer should also be very slow. This is because there is no ternary Sn-Ag-Ni IMC existing in the Sn-Ag-Ni system [19], and the supply of Sn from the ξAg IMC to Ni barrier layer for producing new Ni-Sn IMC is limited.

5. Conclusions

From the above results and discussion for the Ag/Sn/Ag TLP joints used in power die attachment, the following conclusions can be drawn:

1) The thickness of the Ag base metal layers on both the power die and the supporting substrate should be at least two times of the average thickness that is required to consume the Sn interlayer for producing Ag_3Sn IMC. Otherwise, the Ni barrier layer underneath the original Ag layer will be locally attacked by liquid Sn to react into Ni_3Sn_4 IMC, which may lead to the formation and growth to a chain of voids along the interface between the Ni_3Sn_4 and Ag-Sn IMCs during extended bonding process and/or in service.
2) A thickness of 2 μm to 3 μm for the Sn interlayer in combination with a thickness of 4 μm to 6 μm for the Ag base metal layers deposited on both the semiconductor power die and the supporting substrate will be a suitable selection for producing the Ag/Sn/Ag TLP joints used in power die attachment. Such a combination of Sn interlayer and Ag base metal layers for producing good quality of Ag/Sn/Ag TLP joints has been demonstrated by the results shown in Figs. 6 and 7.
3) The diffusivities of Ag and Sn in ζAg IMC at 250 °C determined from the data fittings of the measured thicknesses of Ag_3Sn IMC and ξAg IMC layers to the simulated results with a numerical method are 5.73×10^{-16} m^2/s and 7.92×10^{-17} m^2/s. They are slightly higher than the volume diffusivities of Ag and Sn in Ag_3Sn IMC, but four to six orders of magnitude lower than the grain-boundary diffusivities of Ag and Sn in Ag_3Sn IMC reported in the existing literature.
4) Simulated results for the evolution of phases in the Ag/Sn/Ag TLP joints indicate that it is more realistic to process the Ag/Sn/Ag TLP joints consisting of major

Ag_3Sn IMC plus minor ξAg IMC and residual Ag for power die attachment. The Ag/Sn/Ag TLP joints can be expected to consist of major ξAg IMC plus residual Ag during the majority of service lifetime if the Ag/Sn/Ag TLP joints are applied in power die attachment.

Acknowledgements

This research was supported by the UK Engineering and Physical Science Research Council as part of the Innovative Electronic Manufacturing Research Centre (IeMRC) [grant number EP/H03014X/1] and the European Commission through the Seventh Research Framework Programme, CleanSky "Systems for Green Operations".

Reference

[1] L. Bernstein, J. Electrochem. Soc. 113(12), 1282 (1966).

[2] C.C. Lee, C.Y. Wang, Thin Solid Films 208, 202 (1992).

[3] G.S. Matijasevic, C.C. Lee, C.Y. Wang, Thin Solid Films 223, 276 (1993).

[4] G. Humpston, D.M. Jacobson, Principles of Soldering (Materials Park, Ohio 44073-0002, ASM International, 2004), pp. 230-235.

[5] J.F.Li, P.A. Agyakwa, C.M Johnson, Acta Mater. 58(9), 3429 (2010).

[6] J.F.Li, P.A. Agyakwa, C.M Johnson, Acta Mater. 59(3), 1198 (2011).

[7] D. E. Crees, G. Humpston, D.M. Jacobson, D. Newcombe, GEC J. Res. 6(2), 71 (1988).

[8] T.B. Wang, Z.Z. Shen, R.Q. Ye, X.M. Xie, F. Stubhan, J. Freytag, J. Electron. Mater. 29(4), 443 (2000).

[9] F. Bartels, J.W. Morris, G. Dalke, W. Gust, J. Electron. Mater. 23(8), 787 (1994).

[10] E. Lugscheider, K. Bobzin, M.K. Lake, Surf. Coat. Technol. 142-144, 813 (2001).

[11] N.S. Bosco, F.W. Zok, Acta Mater. 53(7), 2019 (2005).

[12] E. Lugscheider, K. Bobzin, M. Maes, S. Ferrara, A. Erdle, Surf. Coat. Technol. 200(1-4), 444 (2005).

[13] S. Sommadossi, W. Gust, E.J. Mittemeijer, Mater. Chem. Phys. 77(3), 924 (2002).

[14] P.K. Khanna, G. Dalke, W. Gust, Z. Metallkd. 90(9), 722 (1999).

[15] N. Quitoriano, W.S. Wong, L. Tsakalakos, Y. Cho, T. Sands, J. Electron. Mater. 30(11), 1471 (2001).

[16] T. Studnitzky, R. Schmid-Fetzer, J. Electron. Mater. 32(2),70 (2003).

[17] K. Guth, N. Oeschler, L. Bower, R. Speckels, G. Strotman, N. Heuck, S. Krasel, A. Ciliox, in Proceedings of 7th International Conference on Integrated Power Electronics Systems, March 6-8, 2012, Nuremberg, Germany, pp. 380-384.

[18] "Binary Ag-Sn phase diagram," Facility for the Analysis of Chemical Thermodynamics (FACT), Available from: http://www.crct.polymtl.ca/FACT/phase_diagram.php?file=Ag-Sn.jpg&dir=SGTE.

[19] H.F. Hsu, S.W. Chen, Acta Mater. 52, 2541 (2004).

[20] G. Ghosh, J. Appl. Phys. 88, 6887 (2000).

[22] V. Tikare, J.D. Cawley, Acta Mater. 46, 1333 (1998).

[23] Z. Mei, A.J. Sunwoo, J.W. Morris Jr., Metall. Trans. A23, 857 (1992).

[21] G. Ghosh, Acta Mater. 49, 2609 (2001).

[24] J.F.Li, P.A. Agyakwa, C.M Johnson, J. Mater. Sci. 45, 2340 (2010).

[25] J.F.Li, P.A. Agyakwa, C.M Johnson, Intermetallics 40, 50 (2013).

[26] H.W. King, T.B. Massalski, Phil. Mag. 6, 669 (1961).

[27] W. Klement Jr., Transactions of the Metallurgical Society of Aime 233, 1182 (1965).

[28] R.H. Kane, B.C. Giessen, N.J. Grant, Acta Metall. 14, 605 (1966).

[29] C.W. Fairhurst, J.B. Cohen, Acta Crystallogr. B28, 371 (1972).

[30] S. Barat, J.K. Mukherjee, Indian J. Technol. 13, 510, (1975).

[31] Y. Ning; X. Zhou, J. Alloys Compd. 182, 131 (1992).

[32] E. Roennebro, J. Yin, A. Kitano, M. Wada, T. Sakai, Solid Stat. Ion. 176, 2749 (2005).

[33] T. Okabe, R.F. Hochman, M.E. Mclain, J. Biomed. Res. 8, 381 (1974).

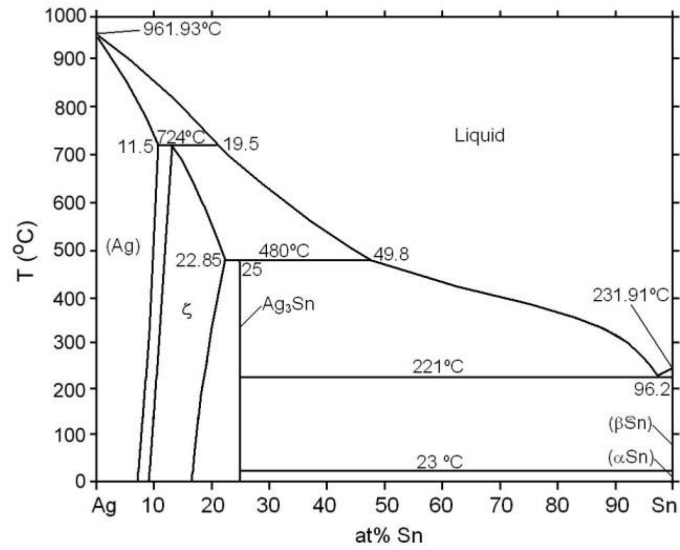

Fig. 1. Phase diagram of binary Ag-Sn system.

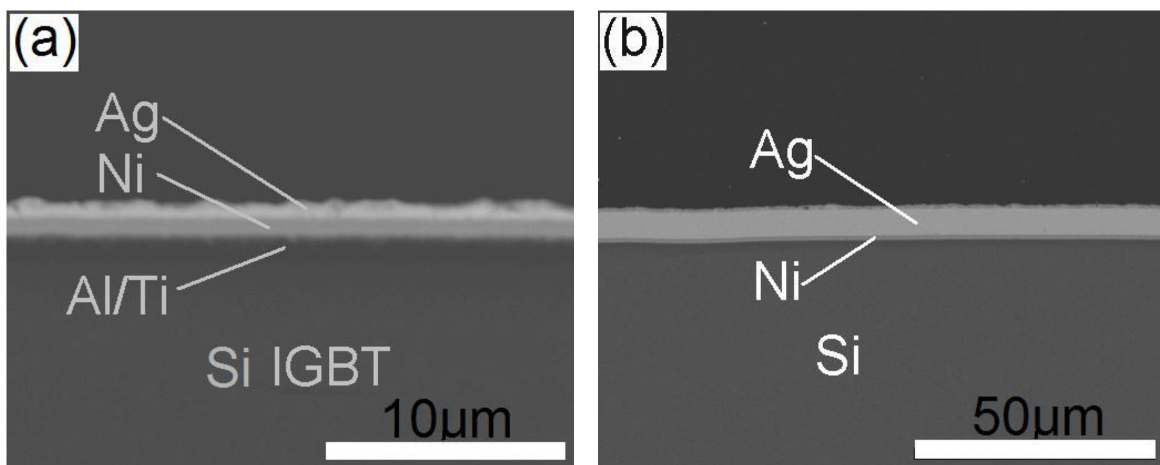

Fig. 2. SEM images taken from the polished cross sections of: (a) real IGBT with conventional Ni\Ag metallization; and (b) dummy Si chip with thickened Ni\Ag metallization.

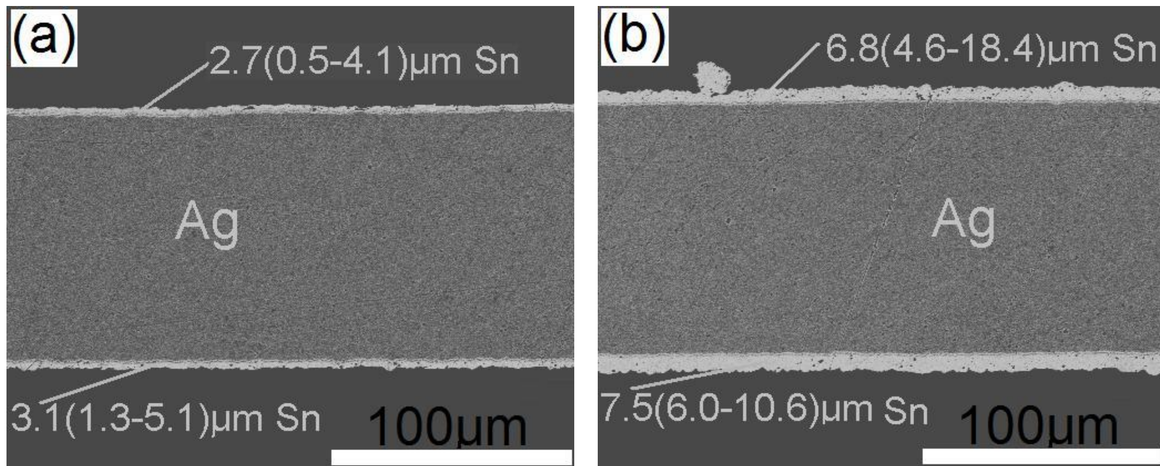

Fig. 3. SEM images taken from the polished cross sections of 100 μm thick Ag foil electroplated with: (a) 2.7 μm thick Sn; and (b) 6.8 μm thick Sn.

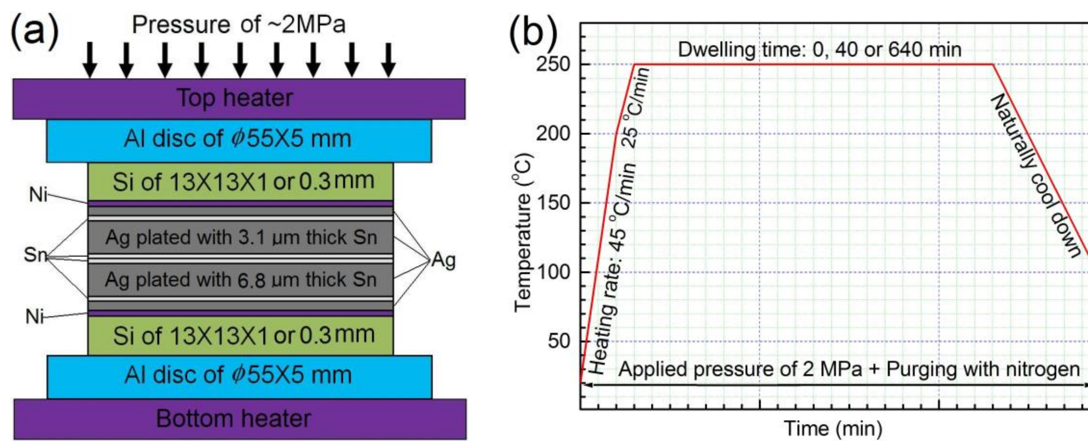

Fig. 4. Schematic: (a) sample geometry; and (b) temperature/pressure profile used to join both real and dummy Si die on Ag foils electroplated with 2.7 μm and 6.8 μm thick Sn. Note that the dimensions of the different components are not to scale.

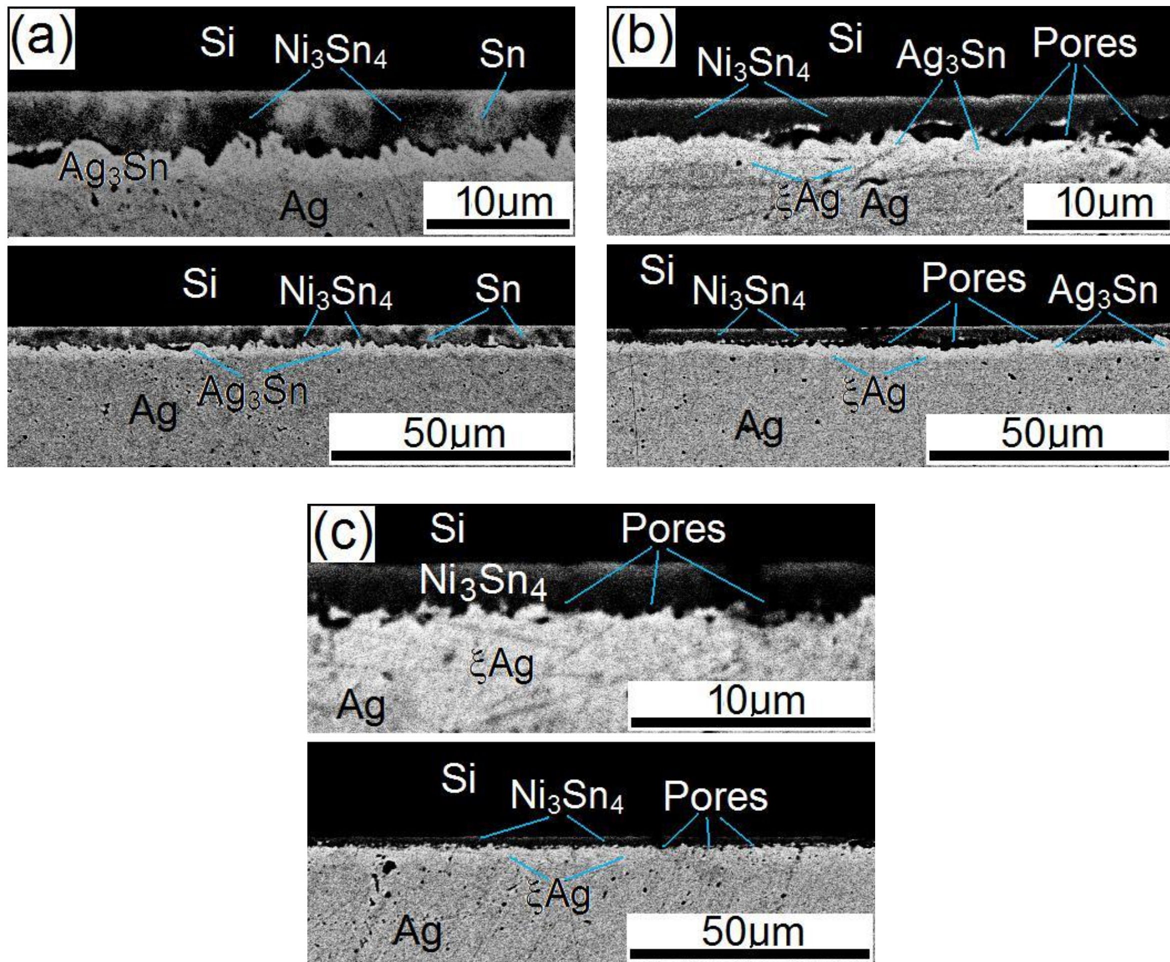

Fig. 5. SEM images taken from the polished cross sections of the samples of real Si IGBTs with conventional Ni\Ag metallization on 100 μm thick Ag foil electroplated with 2.7 μm thick Sn at 250°C and 2MPa for: (a) sample A0, 0 min; (b) sample A1, 40 min; and (c) sample A2, 640min.

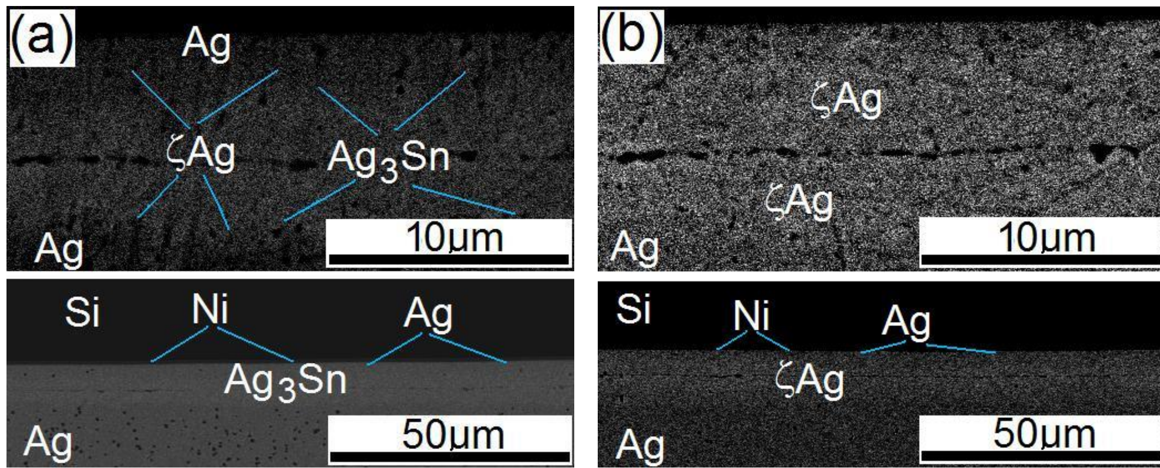

Fig. 6. SEM images taken from the polished cross sections of the samples of dummy Si chips with thickened Ni\Ag metallization on 100 µm thick Ag foil electroplated with 2.7 µm thick Sn at 250°C and 2MPa for: (a) sample C1, 40 min; and (b) sample C2, 640min.

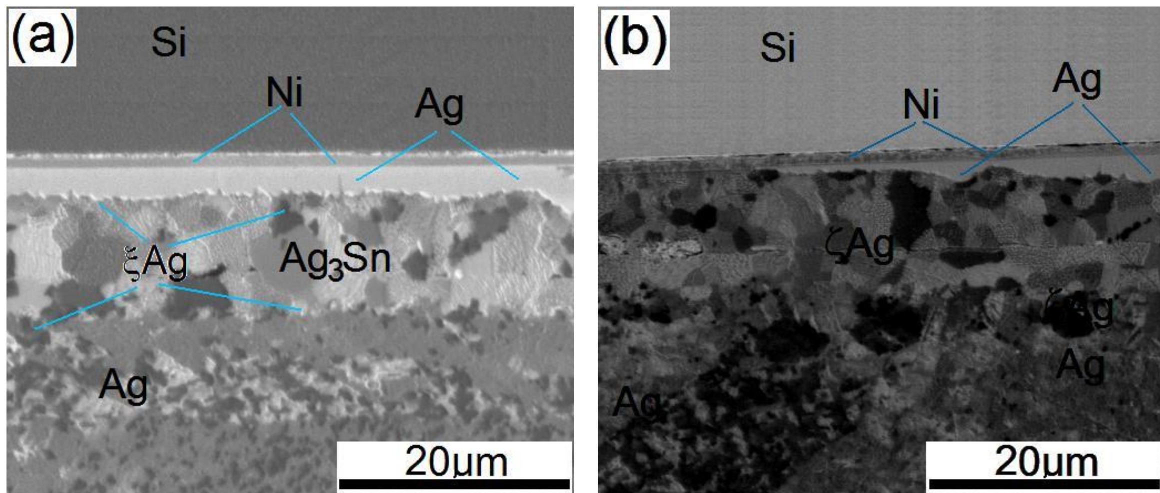

Fig. 7. FIB images taken from the polished cross sections of the samples of dummy Si chips with thickened Ni\Ag metallization on 100 µm thick Ag foil electroplated with 2.7 µm thick Sn at 250°C and 2MPa for: (a) sample C1, 40 min; and (b) sample C2, 640min.

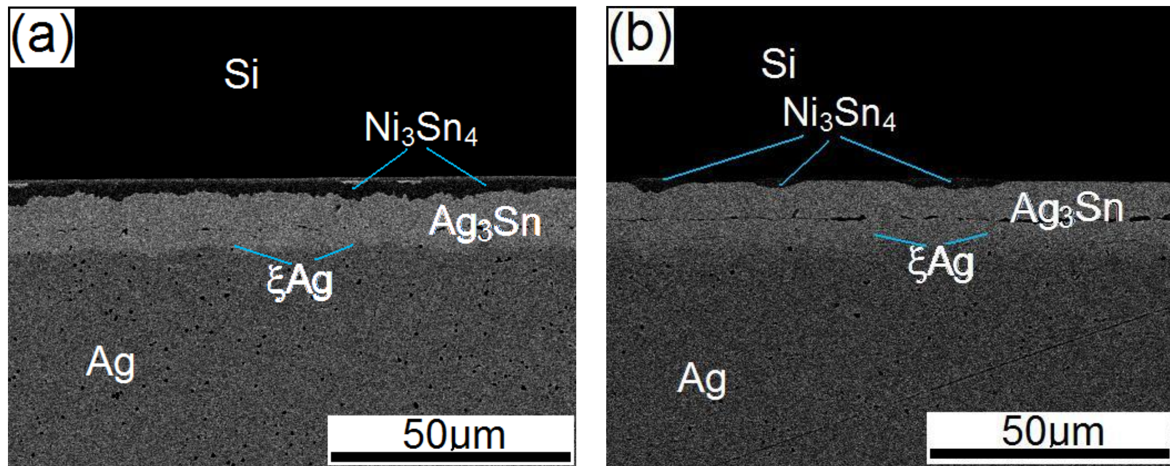

Fig. 8. SEM images taken from the polished cross sections of the samples of dummy Si chips with thickened Ni\Ag metallization on 100 μm thick Ag foil electroplated with 6.8 μm thick Sn at 250°C and 2MPa for: (a) sample D1, 40 min; and (b) sample D2, 640min.

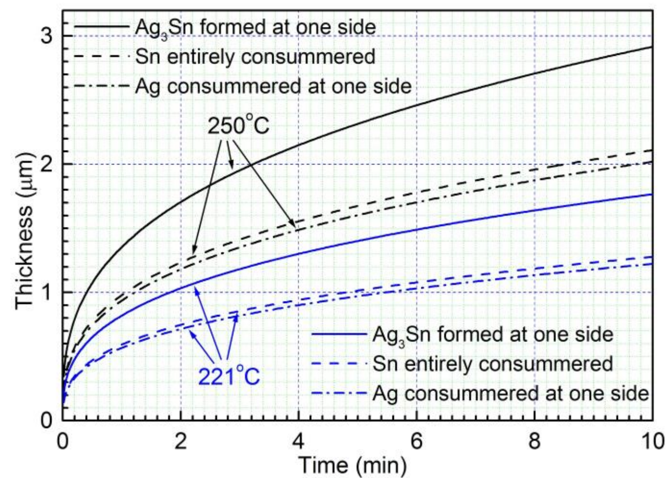

Fig. 9. The growth of the Ag_3Sn IMC and the consumptions of the Ag base metal layers and the Sn interlayer in the Ag/Sn/Ag TLP samples during the early bonding stage for bonding temperatures of 221 ℃ and 250 ℃, which are calculated with Eqs. (1) and (2).

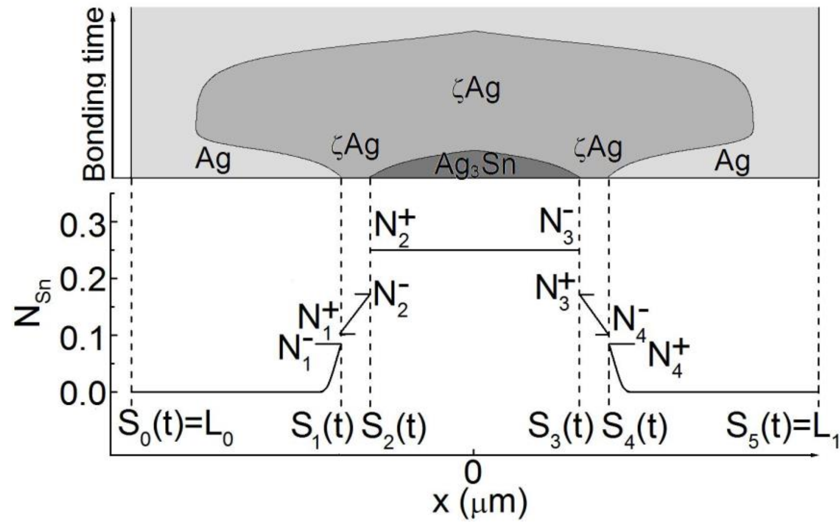

Fig. 10. Schematic illustration of one-dimensional distribution of Molar fraction N_{Sn} across one Ag/Sn/Ag TLP joint at the instant time of t_0 after the Sn interlayer is consumed fully.

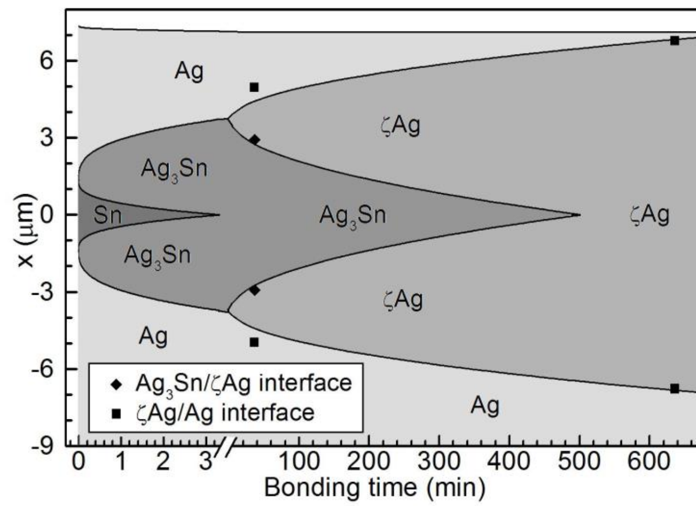

Fig. 11. Data fittings of the measured thicknesses of Ag_3Sn and ξAg layers in the samples C1 and C2 (solid points) to those simulated using the numerical method to solve Eqs. (1) to (7).

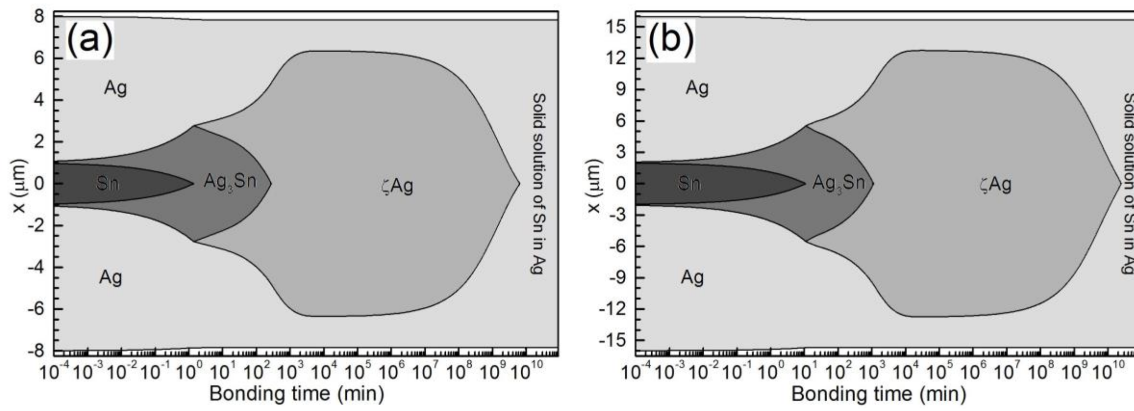

Fig. 12. Simulated growth and evolution of phases in the Ag/Sn/Ag TLP joints during extended bonding process at 250 °C: (a) 2 μm thick Sn interlayer sandwiched between two layers of 7 μm thick Ag base metal; and (b) 4 μm thick Sn interlayer sandwiched between two layers of 14 μm thick Ag base metal.

Table I Sample codes and the corresponding Si die, Ag foils and dwelling times used during the bonding process

Code	Thickness of Ag on Si dice (μm)	Thickness of Sn on Ag foil (μm)	Dwelling time (min)
A0	0.7	2.7	0
A1	0.7	2.7	40
A2	0.7	2.7	640
B0	0.7	6.8	0
B1	0.7	6.8	40
B2	0.7	6.8	640
C1	6.0	2.7	40
C2	6.0	2.7	640
D1	6.0	6.8	40
D2	6.0	6.8	640

Table II Results of thickness measurements for the total Ag-Sn IMCs formed in all the bonded samples using the image analysis method

Code	Mean (μm)	Std. Dev. (μm)	Min (μm)	Max (μm)	Ag-Sn IMCs
A0	2.2	0.6	0.7	4.4	Ag_3Sn
A1	2.0	0.4	0.7	3.2	Ag_3Sn + ξAg
A2	3.6	0.6	2.3	5.1	ξAg
B0	2.0	0.6	0.5	3.8	Ag_3Sn
B1	1.7	0.4	0.2	3.2	Ag_3Sn + ξAg
B2	3.8	0.6	2.3	5.5	ξAg
C1	9.9	0.6	8.3	12.0	Ag_3Sn + ξAg
C2	13.5	0.7	12.1	15.1	ξAg
D1	11.2	1.0	7.4	13.1	Ag_3Sn + ξAg
D2	11.3	0.7	9.6	13.4	Ag_3Sn + ξAg

Table III The values used in the present numerical simulation for the Molar fraction of Sn, density and Molar volume of the different phases and interfaces in Ag/Sn/Ag TLP joints, which were calculated based on the binary Ag-Sn phase diagram and the lattice cell parameters reported in Refs. [24-31]

Phase	Ag	Ag	ζAg	ζAg	Ag_3Sn	Sn
Interface		Ag/ζAg	Ag/ζAg	ζAg/Ag_3Sn	ζAg/Ag_3Sn	
Molar fraction of Sn	0	0.085	0.103	0.173	0.250	1
Density (g/cm^3)	10.49	10.39	10.31	10.11	9.92	7.36
Molar volume (cm^3/mol)	10.28	10.47	10.56	10.86	11.14	16.12

Table IV The diffusivities of Ag and Sn in Ag calculated from Arrhenius-type plots assessed in Ref. [21] and those in ζAg IMC extracted in this study

	Diffusivity at 250°C (m^2/s)	Reference
Ag in Ag	3.72×10^{-23}	Calculated from data in Ref. [21]
Sn in Ag	1.10×10^{-21}	Calculated from data in Ref. [21]
Ag in ζAg	5.73×10^{-16}	Extracted in this study
Sn in ζAg	7.92×10^{-17}	Extracted in this study